The effect of cyclone inlet dimensions on the flow pattern and performance

Khairy Elsayed *, Chris Lacor

Vrije Universiteit Brussel, Department of Mechanical Engineering, Research Group Fluid Mechanics and Thermodynamics, Pleinlaan 2, 1050 Brussels, Belgium

ARTICLE INFO

ABSTRACT

The effect of the cyclone inlet dimensions on the performance and flow field pattern has been investigated computationally using the Reynolds stress turbulence model (RSM) for five cyclone separators. The results show that, the maximum tangential velocity in the cyclone decreases with increasing the cyclone inlet dimensions. No acceleration occurs in the cyclone space (the maximum tangential velocity is nearly constant throughout the cyclone). Increasing the cyclone inlet dimensions decreases the pressure drop. The cyclone cut-off diameter increases with increasing cyclone inlet dimension (consequently, the cyclone overall efficiency decreases due to weakness of the vortex strength). The effect of changing the inlet width is more significant than the inlet height especially for the cut-off diameter. The optimum ratio of inlet width to inlet height b/a is from 0.5 to 0.7.

© 2010 Elsevier Inc. All rights reserved.

1. Introduction

In cyclone separators, a strongly swirling turbulent flow is used to separate phases with different densities. The typical geometrical layout of a gas cyclone, used to separate particles from a gaseous stream, depicted in Fig. 1(a), corresponds to the Stairmand high-efficiency cyclone. The tangential inlet generates the swirling motion of the gas stream, which forces particles toward the outer wall where they spiral in the downward direction. Eventually the particles are collected in the dustbin (or flow out through a dipleg) located at the bottom of the conical section of the cyclone body. The cleaned gas leaves through the exit pipe at the top. Swirl and turbulence are the two competing phenomena in the separation process: the swirl induces a centrifugal force on the solids phase which is the driving force behind the separation; turbulence disperses the solid particles and enhances the probability that particles get caught in the exit stream. Both phenomena are related to the particle size, and the flow conditions in the cyclone [1].

While the cyclone geometry is simple, the flow is extremely complicated three dimensional swirling flow. The complexity of the gas solid flow pattern in cyclones has long been a matter of many experimental and theoretical works. At present laser Doppler anemometry (LDA) [e.g. 2,3] and particle image velocimetry (PIV) [e.g. 4–6] are frequently employed to study experimentally the flow structure in the cyclones. As for the theoretical work, computational fluid dynamics (CFD) codes have proven to be a useful tool for simulating cyclonic flows [e.g. 1,7–10]. The geometry of the cyclone affects the flow pattern and performance. The cyclone geometry is described by seven geometrical parameters, viz. the inlet height a, and width b, the vortex finder diameter D_x and length S, cylinder height h, cyclone total height H_t and cone-tip diameter B_c (Fig. 1(a)).

The effects of cyclone inlet section dimensions on the cyclone performance (pressure drop and cut-off diameter) have been reported in many articles. Casal and Martinez-Benet [11] proposed the following empirical formula for the dimensionless pressure drop (Euler number),

---

 * Corresponding author. Tel.: +32 26 29 2368; fax: +32 26 29 2880.
   E-mail address: kelsayed@vub.ac.be (K. Elsayed).

Nomenclature

a	cyclone inlet height [m]
A_i	inlet cross sectional area ($A_i = ab$) [m]
b	cyclone inlet width [m]
B_c	cyclone cone-tip diameter [m]
d_p	particle diameter [m]
D	cyclone body diameter [m]
D_x	cyclone vortex finder diameter [m]
g_i	acceleration due to gravity in i direction [m/s^2]
h	cylindrical part height [m]
H_t	cyclone total height [m]
k	turbulent kinetic energy [m^2/s^2]
K	fluctuating kinetic energy [m^2/s^2]
L_i	distance between the inlet section and the cyclone center [m]
L_e	distance between the outlet section and the cylindrical barrel top [m]
L_n	cyclone natural length [m]
$\overline{P}$	mean pressure [N/m^2]
P	fluctuating kinetic energy production [m^2/s^3]
Q_{in}	gas volume flow rate [m^3/s]
R_{ij}	Reynolds stress tensor [m^2/s^2]
S	vortex finder length [m]
t	flow physical time [s]
t_{res}	flow average residence time [s]
$\overline{u_i}$	mean velocity [m/s]
u_i	flow velocity component in i direction [m/s]
u_i'	fluctuating velocity component in i direction [m/s]
u_{pi}	particle velocity in i direction [m/s]
V	cyclone volume [m^3]
x_i	position [m]

Greek letters

δ_{ij}	Kronecker delta
ε	turbulence dissipation rate [m^2/s^3]
μ	dynamic viscosity [kg/(m s)]
μ_t	turbulent (eddy) viscosity [kg/(m s)]
v	kinematic viscosity ($v = \mu/\rho$) [m^2/s]
v_t	turbulent (eddy) kinematic viscosity ($v_t = \mu_t/\rho$) [m^2/s]
ρ	gas density [kg/m^3]
ρ_p	particle density [kg/m^3]

Dimensionless numbers

C_D	particle drag coefficient
E_u	Euler number
Re_p	relative Reynolds number
S_g	geometrical swirl number

Abbreviations

CFD	computational fluid dynamics
DPM	discrete phase modeling
GLCC	gas liquid cylindrical cyclone separators
LDA	laser Doppler anemometry
LES	large eddy simulation
MM	Muschelknautz method of modeling
PIV	particle image velocimetry
RNG	renormalization group
RSM	Reynolds stress turbulence model

$$E_u = 11.3 \left(\frac{ab}{D_x} \right)^2 + 2.33, \tag{1}$$

implying proportionality with the square of the inlet area. Ramachandran et al. [12] on the other hand proposed,
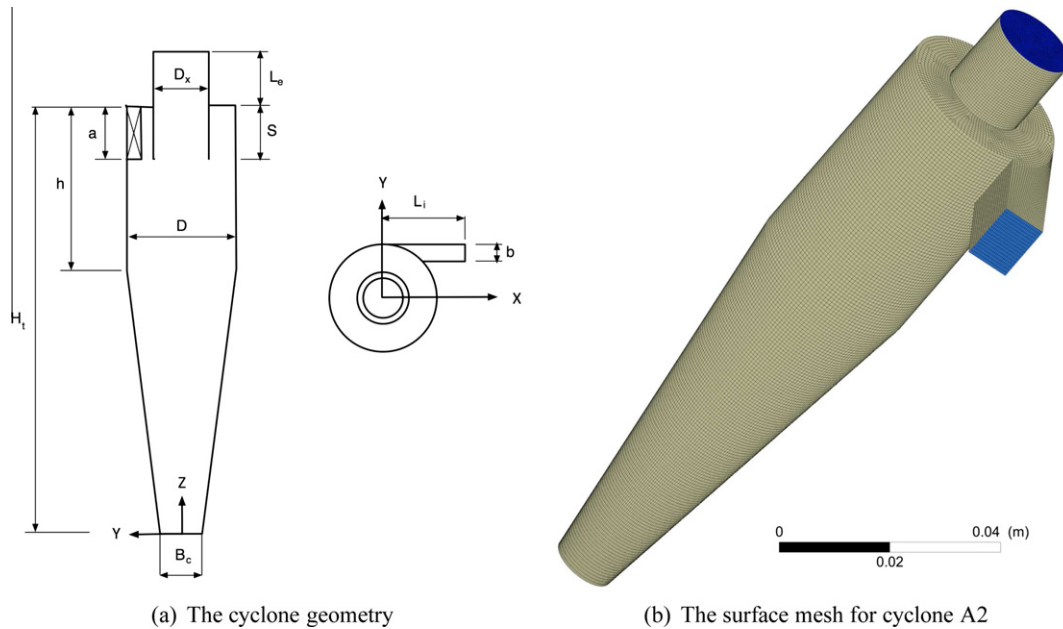
(a) The cyclone geometry   (b) The surface mesh for cyclone A2

Fig. 1. Schematic diagram for Stairmand cyclone separator.

$$E_u = 20 \left(\frac{ab}{D_x^2} \right) \left(\frac{S}{H_t h B_c} \right)^{1/3}, \tag{2}$$

i.e. a linear relation with the inlet area. Iozia and Leith [13,14] presented a correlation to estimate the cut-off diameter d_{50} and found proportionality to $(ab)^{0.61}$. The importance of inlet dimensions becomes clearer after the study of natural length (or vortex length) by several researchers, e.g. Alexander [15]. The cyclone has two spiral motions, outer and inner. In the reverse flow cyclone, the outer vortex weakens and changes its direction at a certain axial distance L_n from the vortex finder [16]. This distance is usually called the turning length, natural length or vortex length of the cyclone. The inlet area is one of the relevant parameters influencing the natural length. Alexander [15] found that L_n decreased proportionally to the inlet area ($A_i = ab$) but the opposite trend has been also reported [16].

Numerous studies have been performed for the effect of geometrical parameters on the flow pattern and performance [e.g. 8,17–20] while the effect of cyclone inlet dimensions remained largely unexplored. The articles investigating the effect of cyclone geometry report only briefly on the effect of inlet section dimensions on the cyclone performance without sufficient details about their effects on the flow pattern and velocity profiles. The new trend is to study the multi-inlet cyclone [e.g. 21–23].

The effects of cyclone inlet on the flow field and performance of cyclone separator have been numerically investigated by Zhao et al. [24]. They compared the performance of two types of cyclones with the conventional single inlet and spiral double inlets using the Reynolds stress turbulence model. The results show that, the new type cyclone separator using the adding spiral double inlet can improve the symmetry of gas flow pattern and enhance the particle separation efficiency. While their finding is for double inlets cyclone, but it support the importance of the effect of the inlet section dimensions on the performance of cyclone separator.

The significant effects of the cyclone inlet dimensions on the cyclone performance have been acknowledged in many articles [e.g. 25]. For two inlets cyclone separators, Zhao [26] reported the possibility of increasing the cyclone efficiency without significantly increasing the pressure drop by improving the inlet geometry of the cyclone. The effect of inlet section angle has been tested by many researchers. Qian & Zhang [27] computationally investigated the effect of the inlet section angle. The pressure drop of the cyclone decreases to 30% lower value than that for conventional cyclone, if θ becomes 45°, where θ is the inlet section angle. However, Qian & Wu [28] reported only 15% reduction in the pressure drop for $\theta = 45°$.

The significant effect of the inlet section configuration on the performance of other highly swirling equipment (e.g., the gas liquid cylindrical cyclone separators (GLCC)) has been also reported. Movafaghian et al. [29] studied the effect of the inlet geometry on the hydrodynamics of two phase flow in GLCC. They compared two GLCC separators, one with singe inlet and the other with dual inlet configuration. They found the performance of dual inlet is superior with respect to the single inlet GLCC separators. However, they did not study the effects of the inlet section dimensions. Also Erdal & Shirazi [30] investigated the effect of three different inlet geometries (one inclined inlet, two inclined inlets and a gradually reduced inlet nozzle) on the flow behavior. They reported that, the gradually reduced inlet nozzle geometry is the preferred geometry.

In summary, all articles mentioned above did not study the effect of inlet height or width dimensions on the performance and flow pattern but they studied the effect of inlet configurations (inclined instead of tangential), or the effect of number of inlets (single or double) or the shape of the inlet section (rectangular duct or nozzle).

The present study is intended to computationally investigate using the Reynolds stress turbulence model (RSM) the effect of increasing the cyclone inlet width and height on the pressure drop and cut-off diameter and obtaining more details about the flow field pattern and velocity profiles.

2. Description of the numerical model

2.1. Selection of the turbulence model

For the turbulent flow in cyclones, the key to the success of CFD lies with the accurate description of the turbulent behavior of the flow [7]. To model the swirling turbulent flow in a cyclone separator, there are a number of turbulence models available in FLUENT. These range from the standard $k - \varepsilon$ model to the more complicated Reynolds stress turbulence model (RSM). Also large eddy simulation (LES) methodology is available as an alternative to the Reynolds averaged Navier–Stokes approach.

Selection of a suitable turbulence model for the highly swirling flows has been investigated by many researchers [e.g. 7,31–43].

The standard $k - \varepsilon$, RNG $k - \varepsilon$ and Realizable $k - \varepsilon$ models were not optimized for strongly swirling flows found in cyclone separators [37,40]. Both the standard $k - \varepsilon$ and RNG $k - \varepsilon$ turbulence models give unrealistic distribution for the axial velocity profiles (upward flow close to the wall) [31,42]. Only the Reynolds stress turbulence model (RSM) is capable of predicting the combined vortex in accordance with the experimental data [31,42]. The successful application of the RSM turbulence model for different studies in cyclone separators has been reported by many researchers [e.g. 34,37,24,44,45,8,9]. Also its successful applications in the most recent cyclone separators studies have been reported in many articles [e.g. 46–48,10,49]

The Reynolds stress turbulence model (RSM) requires the solution of transport equations for each of the Reynolds stress components. It yields an accurate prediction on the swirl flow pattern, axial velocity, tangential velocity, cut-off diameter and pressure drop in cyclone simulations [50,31,42,10]. It will be used in this study to reveal the effect of changing the cyclone inlet dimensions on the turbulent flow in the cyclone separator.

2.2. The governing equations

2.2.1. Navier–Stokes equations
For an incompressible fluid flow, the equation for continuity and balance of momentum are given as [47]:

$$\frac{\partial \overline{u_i}}{\partial x_i} = 0, \tag{3}$$

$$\frac{\partial \overline{u_i}}{\partial t} + \overline{u_j} \frac{\partial \overline{u_i}}{\partial x_j} = -\frac{1}{\rho} \frac{\partial \overline{P}}{\partial x_i} + v \frac{\partial^2 \overline{u_i}}{\partial x_j \partial x_j} - \frac{\partial}{\partial x_j} R_{ij}, \tag{4}$$

where $\overline{u_i}$ is the mean velocity, x_i is the position, $\overline{P}$ is the mean pressure, ρ is the gas density, v is the gas kinematic viscosity, and $R_{ij} = \overline{u_i' u_j'}$ is the Reynolds stress tensor. Here, $u_i' = u_i - \overline{u_i}$ is the ith fluctuating velocity component.

The RSM turbulence model provides differential transport equations for evaluation of the turbulence stress components (Eq. (5)).

$$\frac{\partial}{\partial t} R_{ij} + \overline{u_k} \frac{\partial}{\partial x_k} R_{ij} = \frac{\partial}{\partial x_k} \left(\frac{v_t}{\sigma^k} \frac{\partial}{\partial x_k} R_{ij} \right) - \left[R_{ik} \frac{\partial \overline{u_j}}{\partial x_k} + R_{jk} \frac{\partial \overline{u_i}}{\partial x_k} \right] - C_1 \frac{\varepsilon}{K} \left[R_{ij} - \frac{2}{3} \delta_{ij} K \right] - C_2 \left[P_{ij} - \frac{2}{3} \delta_{ij} P \right] - \frac{2}{3} \delta_{ij} \varepsilon, \tag{5}$$

where the turbulence production terms P_{ij} are defined as [47]:

$$P_{ij} = -\left[R_{ik} \frac{\partial \overline{u_j}}{\partial x_k} + R_{jk} \frac{\partial \overline{u_i}}{\partial x_k} \right], \quad P = \frac{1}{2} P_{ij} \tag{6}$$

With P being the fluctuating kinetic energy production. μ_t is the turbulent (eddy) viscosity; and $\sigma^k = 1$, $C_1 = 1.8$, $C_2 = 0.6$ are empirical constants The transport equation for the turbulence dissipation rate, ε, is given as [51]:

$$\frac{\partial \varepsilon}{\partial t} + \overline{u_j} \frac{\partial \varepsilon}{\partial x_j} = \frac{\partial}{\partial x_j} \left[\left(v + \frac{v_t}{\sigma^\varepsilon} \right) \frac{\partial \varepsilon}{\partial x_j} \right] - C^{\varepsilon 1} \frac{\varepsilon}{K} R_{ij} \frac{\partial \overline{u_i}}{\partial x_j} - C^{\varepsilon 2} \frac{\varepsilon^2}{K}. \tag{7}$$

In Eq. (7), $K = \frac{1}{2} \overline{u_i' u_i'}$ is the fluctuating kinetic energy, and ε is the turbulence dissipation rate. The values of constants are $\sigma^\varepsilon = 1.3$, $C^{\varepsilon 1} = 1.44$ and $C^{\varepsilon 2} = 1.92$.

2.3. Discrete phase modeling (DPM)

The Lagrangian discrete phase model in FLUENT follows the Eulerian–Lagrangian approach. The fluid phase is treated as a continuum by solving the time-averaged Navier–Stokes equations, while the dispersed phase is solved by tracking a large

number of particles through the calculated flow field. The dispersed phase can exchange momentum, mass, and energy with the fluid phase.

A fundamental assumption made in this model is that the dispersed second phase occupies a low volume fraction (usually less than 10–12%, where the volume fraction is the ratio between the total volume of particles and the volume of fluid domain), even though high mass loading is acceptable. The particle trajectories are computed individually at specified intervals during the fluid phase calculation. This makes the model appropriate for the modeling of particle-laden flows. The particle loading in a cyclone separator is small (3–5%), and therefore, it can be safely assumed that the presence of the particles does not affect the flow field (one-way coupling) [10].

In terms of the Eulerian–Lagrangian approach (One Way coupling), the equation of particle motion is given by [24]

$$\frac{du_{pi}}{dt} = \frac{18\mu}{\rho_p d_p^2} \frac{C_D Re_p}{24} (u_i - u_{pi}) + \frac{g_i(\rho_p - \rho)}{\rho_p}, \tag{8}$$

$$\frac{dx_{pi}}{dt} = u_{pi}, \tag{9}$$

where the term $\frac{18\mu}{\rho_p d_p^2} \frac{C_D Re_p}{24} (u_i - u_{pi})$ is the drag force per unit particle mass [24]. ρ and μ are the gas density and dynamic viscosity respectively, ρ_p and d_p are the particle density and dimeter respectively, C_D is the drag coefficient, u_i and u_{pi} are the gas and particle velocity in i direction respectively, g_i is the gravitational acceleration in i direction, Re_p is the relative Reynolds number.

$$Re_p = \frac{\rho_p d_p |u - u_p|}{\mu}. \tag{10}$$

In FLUENT, the drag coefficient for spherical particles is calculated by using the correlations developed by Morsi and Alexander [52] as a function of the relative Reynolds numbers Re_p. The equation of motion for particles was integrated along the trajectory of an individual particle. Collection efficiency statistics were obtained by releasing a specified number of mono-dispersed particles at the inlet of the cyclone and by monitoring the number escaping through the outlet. Collisions between particles and the walls of the cyclone were assumed to be perfectly elastic (coefficient of restitution is equal to 1).

2.4. Boundary conditions

A velocity inlet boundary condition is used at the cyclone inlet, meaning that a velocity normal to the inlet is specified. An outflow boundary condition is used at the outlet. The no slip boundary condition is used at the other boundaries. The air volume flow rate Q_{in} = 50 L/min for all cyclones, air density 1.0 kg/m^3 and dynamic viscosity of 2.11E−5 Pa s. The turbulent intensity equals 5% and characteristic length equals 0.07 times the inlet width [31].

2.5. Configuration of the five cyclones

The numerical simulations were performed on five cyclones with different inlet dimensions. Fig. 1(a) and Table 1 give the cyclones dimensions. Table 2 gives more details for the used cyclones including the number of cells, geometric swirl number, cyclone volume, flow residence time and the inlet velocity for each cyclone.

In swirling flow, the swirl number usually characterizes the degree of swirl. In cyclone separators, the swirling flow is characterized by the geometric swirl number. The geometric swirl number S_g is a measure for the ratio of tangential to axial momentum [1,53], defined by [31]

Table 1
The geometrical dimensions of the tested cyclones[a].

Dimension		Cyclone[b]	Dimension/D	b/a
Gas outlet diameter, D_x			0.5	
Vortex finder insertion length, S			0.5	
Cone tip-diameter, B_c			0.375	
Cylinder height, h			1.5	
Cyclone height, H_t			4.0	
		A1	0.25	1.05
Inlet height, a	b/D = 0.2625	**A2**	0.375	0.7
		A3	0.50	0.525
		B1	0.15	0.4
Inlet width, b	a/D = 0.375	**B2**	0.2625	0.7
		B3	0.375	1.0

[a] Body diameter, D = 31 mm. The outlet section is above the cylindrical barrel surface by L_e = 0.5D. The inlet section located at a distance $L_i = D$ from the cyclone center.
[b] Cyclones A2 and B2 are identical.

Table 2
The details of the five tested cyclones.

Cyclone	A1	A2 = B2	A3	B1	B3
Number of cells[a]	705,088	714,029	820,362	706,370	816,714
S_g	5.984	3.989	2.992	6.981	2.793
Cyclone volume $\times 10^5$ [m^3]	6.878	6.95	7.017	6.875	7.012
t_{res} [s]	0.0825	0.0834	0.0842	0.0825	0.0841
Inlet velocity [m/s]	13.214	8.809	6.607	15.416	6.166

[a] The total number of hexahedral cells after the grid independence study.

Table 3
The used numerical settings for the current simulations.

	Pressure discretization	Pressure velocity coupling	Momentum discretization	Turbulent kinetic energy	Turbulent dissipation rate	Reynolds stress
Scheme	PRESTO	SIMPLEC	QUICK	Second order upwind	Second order upwind	First order upwind

$$S_g = \frac{\pi D_x D}{4 A_{in}}, \tag{11}$$

where D_x is the vortex finder diameter, D is the cyclone body diameter, and A_{in} is the inlet cross sectional area. For industrial cyclones, the geometrical swirl number usually varies between 1 and 5 [31]. Table 2 shows that, the tested cyclones cover this range. That means, the obtained results can be applied to the industrial cyclones.

2.6. Selection of the numerical schemes

Kaya & Karagoz [42] investigated the suitability of various numerical schemes in highly complex swirling flows, which occur in tangential inlet cyclones. The presence of high-pressure gradients and double-vortex flow structure requires an efficient algorithm for the pressure computation. The PRESTO (Pressure Staggered Option) pressure interpolation scheme is successful in this respect. Among many schemes, the SIMPLEC (Semi–Implicit Method Pressure-Linked Equations Consistent) algorithm for pressure velocity coupling and the QUICK (Quadratic Upstream Interpolation for Convective Kinetics) scheme for momentum equations give better prediction of experimental data. The optimum choice seems to be the second order for turbulent kinetic energy and the first order for Reynolds stresses. They also stated that, the first and second order upwind schemes for turbulent quantities give almost the same results. The used numerical settings for the current simulations are given in Table 3.

2.7. Selection of the time step

The average residence time in the cyclone is determined from the cyclone dimensions and gas flow rate [54]. The residence time $t_{res} = Q_{in}/V$ where Q_{in} is the gas flow rate and V is the cyclone volume. This value is used to select the time step. The time step for the unsteady simulation should be a tiny fraction of the average residence time [37]. The $t_{res} \approx 0.08$ s (for all tested cyclones) as shown in Table 2. So the time step of 1E−4 is an acceptable value for the current simulation for accurate results and achieve scaled residuals less than 1E−5 for all variables. The selected time step results in an average inlet Courant number of 29.25, 28.88, 21.67, 30.40, 21.45 for cyclones A1, A2, A3, B1 and B3 respectively. But as the solver is a segregated implicit solver, so there is no limitations of Courant number for stability conditions.

2.8. Strategy to reach convergence

With regard to the convergence criteria, two aspects should be considered. Firstly, the scaled residuals should be below 1E−5 (The default convergence criterion of FLUENT is that scaled residuals of all equations fall below 1E−3), while secondly, some representative quantities such as velocity and pressure should be monitored until they are constant [27]. Although the present simulations were conversed at about (t = 1.5 − 1.6 s), they were only terminated at t = 2 s to get more accurate time averaged values. The total CPU running time was about (90 h for each case) on 8 nodes CPU Opteron 64 Linux cluster using FLUENT 6.3.26 finite volume commercial solver. All simulations have been converged with the selected time step of 1E−4 s and the numerical settings given in Table 3.

2.9. CFD grid

Fig. 1(b) shows the surface grid of cyclone A2 used in this study. The hexahedral computational grids were generated using GAMBIT grid generator.

Table 4
The details of the grid independence study for cyclone A2.

Total number of cells	Static pressure drop [N/m²]	Total pressure drop [N/m²]	Cut-off diameter [micron]
490,164	95.99	116.86	0.99
714,029	100.922	121.792	1.0
1,174,029	98.68	119.55	1.02
% Difference [a]	2.73	2.25	2.94

[a] The percentage difference between the coarsest and finest grid.

2.9.1. The grid independence study

The grid independence study has been performed for the five tested cyclones. Three levels of grid for each cyclone have been tested, to be sure that the obtained results are grid independent. For example, three levels of mesh; 490,164, 714,029 and 1,174,029 cells have been used for cyclone A2 (B2). The computational results of the three grid types are presented in Table 4. As seen the maximum difference between the results is less than 5%, so the grid template 490,164 produces grid independent results [48]. It has been observed that even 490,164 grid provides a sufficient grid independency. However, for excluding any uncertainty, computations have been performed using the 714,029 cells grid, where the total number of grid points was not that critical with respect to the computation overhead [55].

3. Validation of the numerical model

3.1. Comparison of experimental and simulation velocities

In order to validate the obtained results, it is necessary to compare the prediction with experimental data. The comparison performed with the measurements of Hoekstra [31] of the Stairmand cyclone using laser Doppler anomemetry (LDA). The present simulation are compared with the measured axial and tangential velocity profiles at an axial station located at 94.25 cm from the cyclone bottom ($D_x/D = 0.5$) as shown in Fig. 2 (cf. Hoekstra [31] for more details about the used cyclone in this validation). The RSM simulation matches the experimental velocity profile with underestimation of the maximum tangential velocity, and overestimation of the axial velocity at the central region. Considering the complexity of the turbulent swirling flow in the cyclones, the agreement between the simulations and measurements is considered to be quite acceptable.

3.2. Comparison of experimental and simulation pressure drops and cut-off diameter

The cyclone pressure drop is calculated as the pressure difference between the inlet and the average pressure across the vortex finder exit [31]. The experimental pressure drop of the cyclone can be calculated by the difference between the pressures at the inlet and outlet [27]. The estimation of the total pressure drop (static pressure plus dynamic pressure) is more accurate as it takes into consideration the change in the flow kinetic energy between the inlet and outlet sections. A comparison of the pressure drops (both, the static and total), the cut-off diameter (at particle density of 2740 kg/m³) obtained from the experimental data [31], CFD prediction is shown in Table 5. Table 5 indicates a very small deviations from the
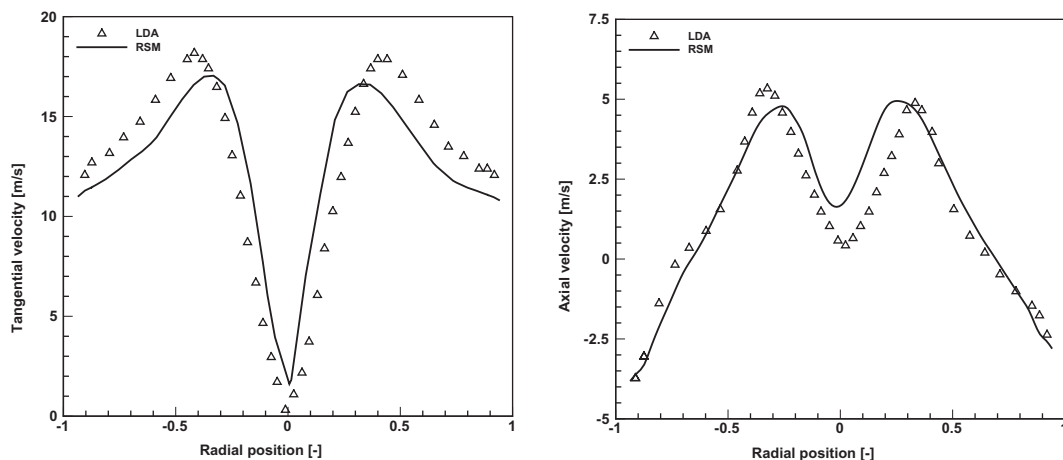

Fig. 2. Comparison of the time averaged tangential and axial velocity between the LDA measurements, Hoekstra [31] and the current Reynolds stress turbulence model (RSM) results at 94.25 cm from the cyclone bottom. From left to right tangential and axial velocity, $D_x/D = 0.5$, The inlet velocity = 10 m/s.

Table 5
Validation of the computational pressure drop and cut-off diameter.

	Static pressure drop [N/m²]	Total pressure drop [N/m²]	Cut-off diameter [micron]
Experimental [31]	300	312.95	1
CFD	309	321.95	0.965
% Error	3	2.876	3.5

experimental values in both the calculated pressure drop and cut-off diameter. As the errors are less than 4%, so it is in the same magnitude as the experimental error [27]. The above comparison results show that the numerical model employed in this study can be used to analyze the gas flow field and performance of the cyclone separator.

4. Results

4.1. The variation of the flow properties in the axial direction

The tangential velocity is the dominant component of the gas flow in cyclones, which results in the centrifugal force for particle separation [44]. Also the development of axial velocity profile in axial direction will be analyzed for the five cyclones. Nine sections are used to plot the velocity profiles as shown in Table 6.

Figs. 3–5 present the radial profiles of the time-averaged static pressure, tangential and axial velocity at 9 axial stations. As expected, the tangential velocity profiles exhibit the so-called Rankine vortex, which consists of two parts, an outer free vortex and an inner solid rotation in the center (Fig. 4). The tangential velocity distribution in the inner region is rather similar at different sections for the same cyclone. In the outer region, due to the sharp drop in velocity magnitude in the near wall region, the distribution is different and the change in the value of maximum tangential velocity is rather limited. Generally, the tangential velocity distribution varies only slightly with axial positions for the same cyclone, which is also reported in other articles [e.g. 2,44,56,57]. This means that, if the tangential velocity increases at one section of the cyclone, it will increase at all other sections. The same conclusion can be drawn from the radial profile of static pressure with higher values of pressure drop expected for cyclone A1 in comparison with cyclones A2 and A3. Cyclone B1 also depicts higher values of pressure in comparison with cyclones B2 and B3 (Fig. 3). The axial velocity profile has the shape of an inverted W for all cyclones except B3 with the shape of an inverted V, as a result of the change in the flow field pattern due to very wide inlet section.

4.2. The effect of cyclone inlet dimensions on the tangential and axial velocity profiles

To evaluate the effect of increasing the cyclone inlet width on the tangential and axial velocity profiles, the tangential and axial velocity profiles at section S9 (close to the inlet section) for the three cyclones (both for A cyclones and B cyclones) are compared in Fig. 6. As is clear from Fig. 6 the variation of axial velocity is limited close to the wall with changing the inlet width or height. The axial velocity profiles for the three cyclones are very similar except at the central region. The most important is the effect of cyclone inlet height or width on the tangential velocity (proportional to the centrifugal force, which is the main force in the separation process). Increasing the cyclone inlet width or height decreases the maximum tangential velocity. Cyclone A1 & B1 have the maximum tangential velocity in comparison with other cyclones. This means that decreasing the cyclone inlet dimension will enhance the collection efficiency.

4.3. The effect of cyclone inlet dimensions on the flow pattern

Fig. 7 shows the contour plots of the time-averaged static pressure, tangential and axial velocity for cyclones A1, A2 and A3. It is observed that, the highest value of the static pressure decreases with increasing the inlet height. The tangential velocity pattern is very similar for all cyclones (Rankine profile). The highest value decreases with increasing the inlet height, so that a better collection efficiency can be expected when decreasing the inlet height. The axial velocity patterns for the three cyclones have the shape of an inverted W profile.

Fig. 8 shows the contour plots of the time-averaged static pressure, tangential and axial velocity for cyclones B1, B2 and B3. It can be seen that, the non-symmetry of the flow increases with increasing the inlet width. The highest value of the static pressure decreases with increasing the inlet width. The tangential velocity pattern is very similar for all cyclones (Rankine

Table 6
The position of different plotting sections[a].

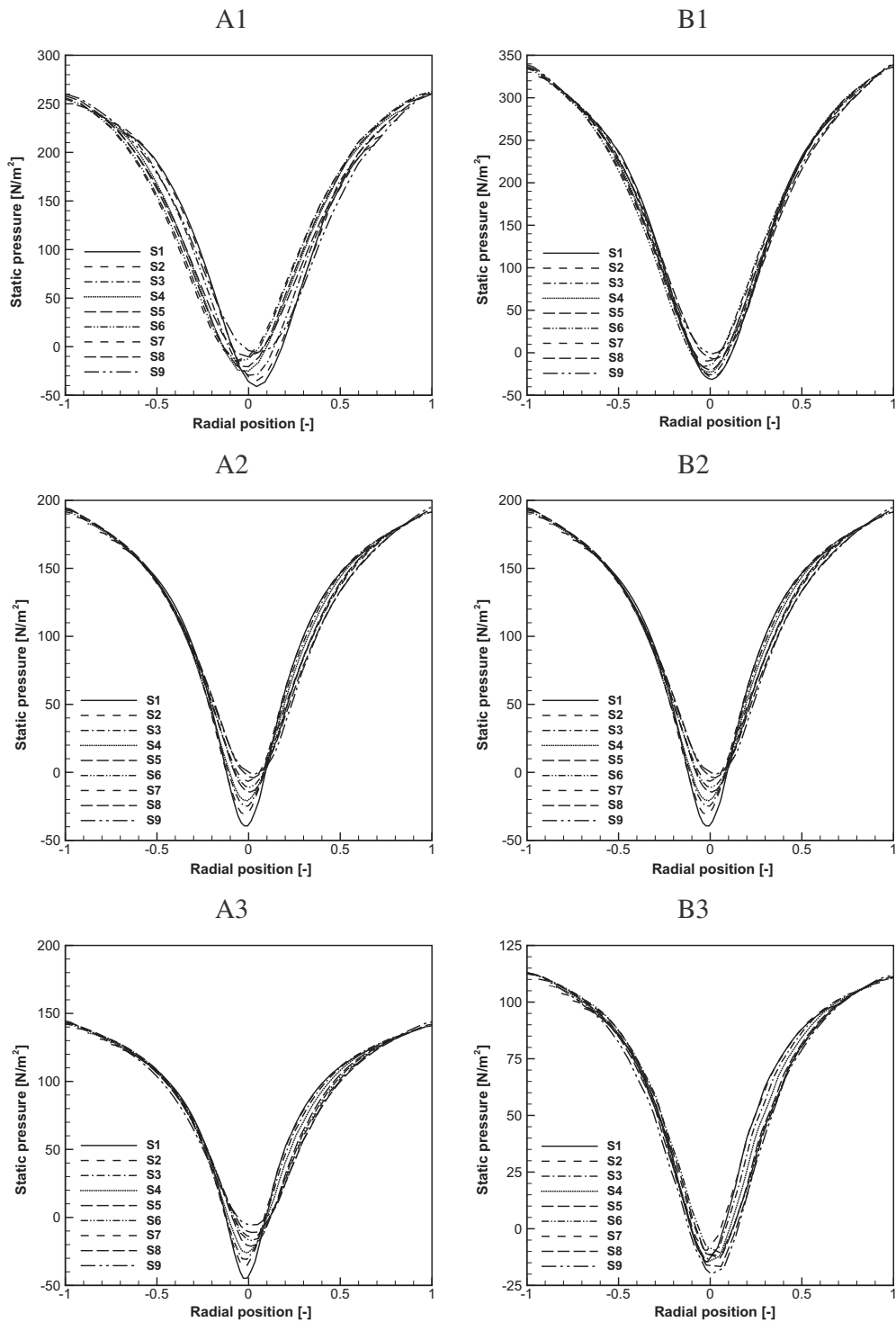| Section	S1	S2	S3	S4	S5	S6	S7	S8	S9
z′/D	2.75	2.5	2.25	2	1.75	1.5	1.25	1.0	0.75

[a] z′ measured from the inlet section top.

Fig. 3. The radial profile for the time-averaged static pressure at different sections. (Note A2 = B2).

profile). The highest value decreases with increasing the inlet width, so that a better collection efficiency can be expected when decreasing the inlet width. The axial velocity patterns for cyclones B1 and B2 have the shape of an inverted W profile while that of cyclone B3 has an inverted V profile. In cyclone B3, the inlet width $b/D = 0.375$ is wider than the gap between the cyclone barrel and the vortex finder wall. As a result some part of the incoming flow will impact the vortex finder and hence will not experience any swirling motion around the vortex finder. This results in different axial velocity profile in
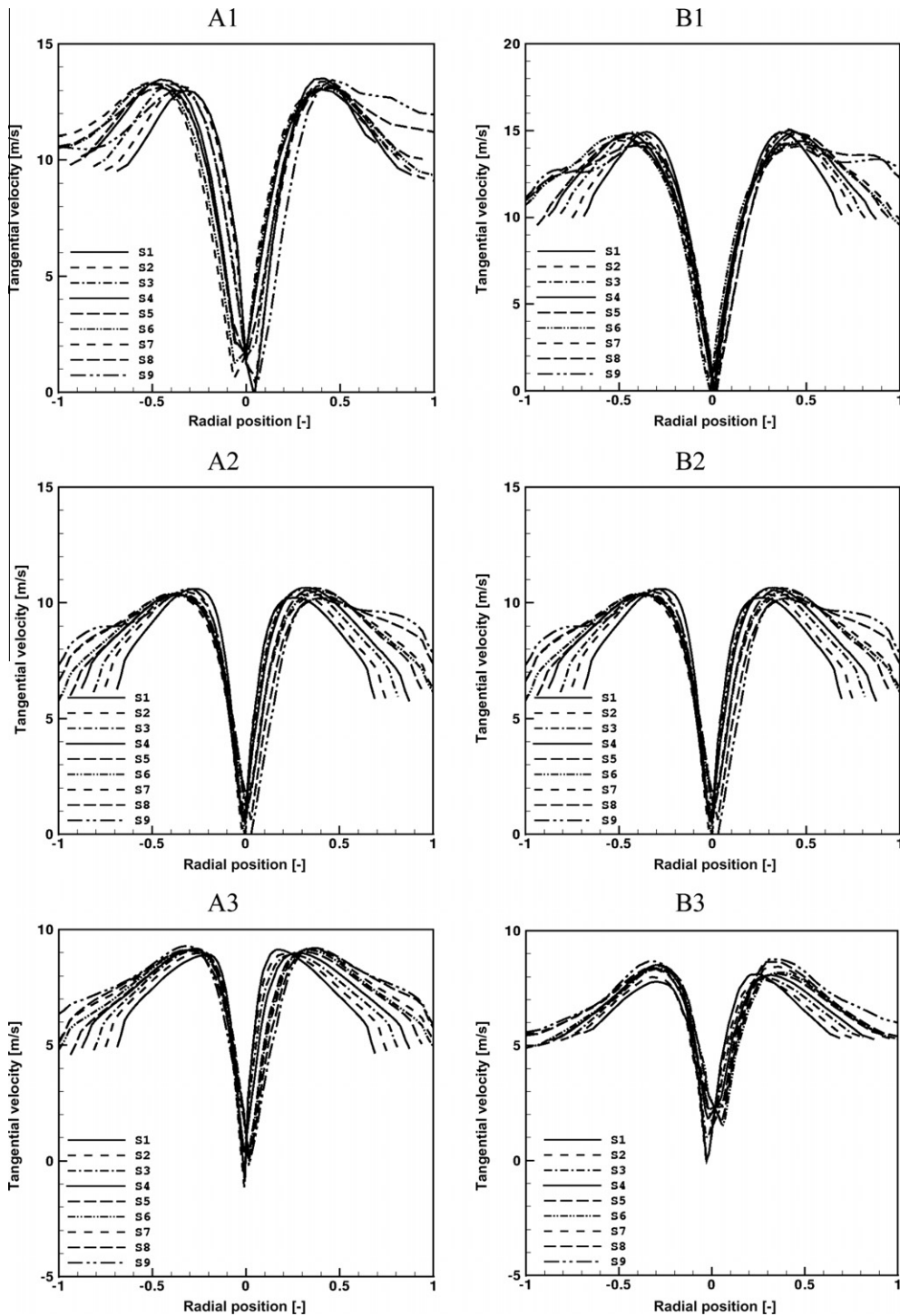
Fig. 4. The radial profile for the time-averaged tangential velocity at different sections. (Note A2 = B2).

cyclone B3 in comparison with the other two cyclones. Furthermore, this will cause excessive stresses on the vortex finder, vibrations and noise).

4.4. The effect of cyclone inlet dimensions on the performance

In order to estimate the effect of cyclone inlet dimensions on the performance parameters, the grade efficiency curves (cut-off diameter), pressure drop have been calculated and presented in Figs. 9 and 10. A discrete phase modeling (DPM)
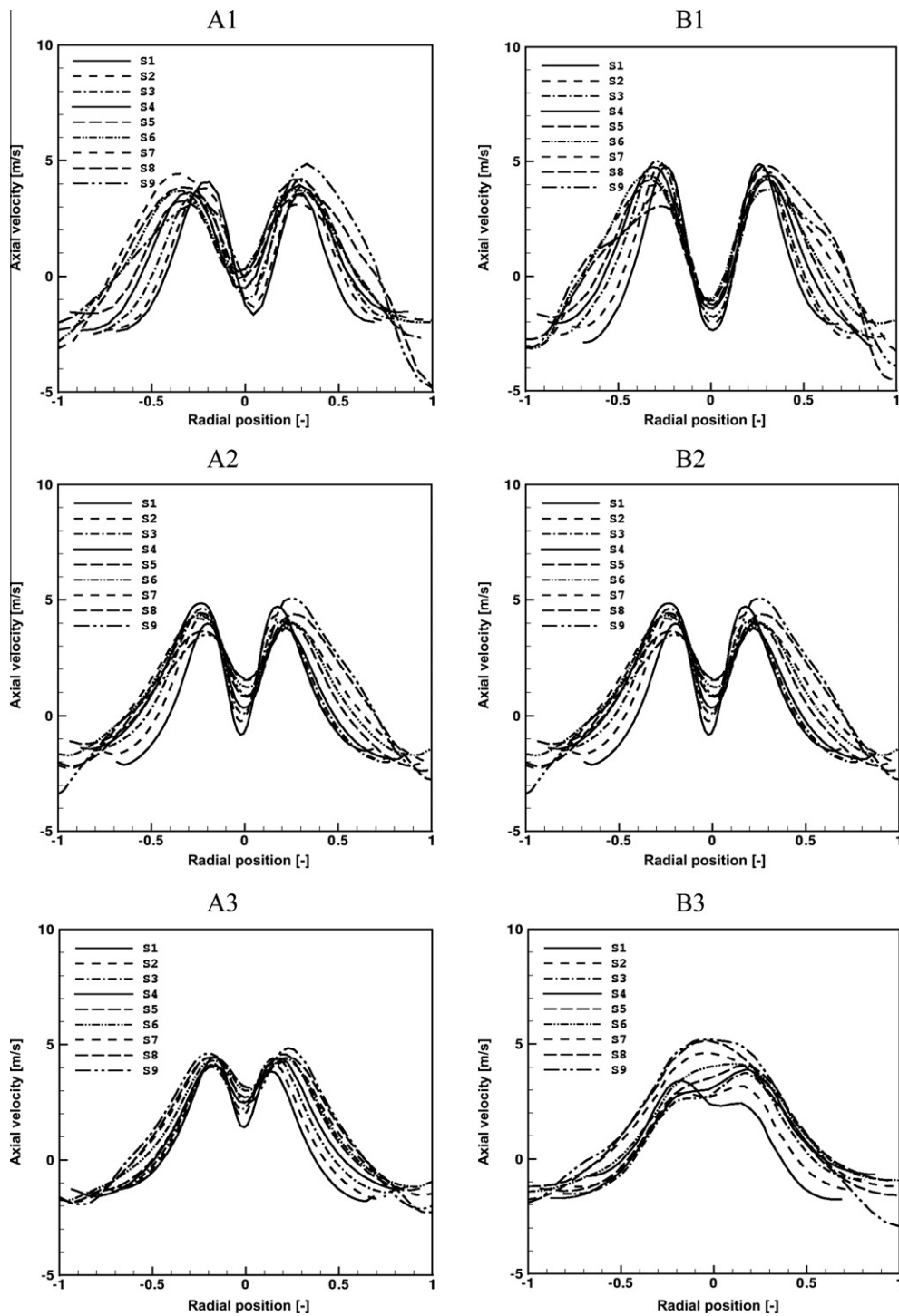
Fig. 5. The radial profile for the time-averaged axial velocity at different sections. (Note A2 = B2).

study has been performed by injecting 10^4 particles from the inlet surface with a particle density of 860 kg/m^3 and with a particle size ranging from 0.025 to 5 μm.

4.4.1. The effect of cyclone inlet height

Fig. 10 shows a rapid decrease in the pressure drop when increasing the inlet height for $0.25 \leqslant a/D \leqslant 0.4$ and a smaller decrease for $a/D \geqslant 0.4$. This behavior can be explained as follows. The pressure drop in the cyclone is composed of three
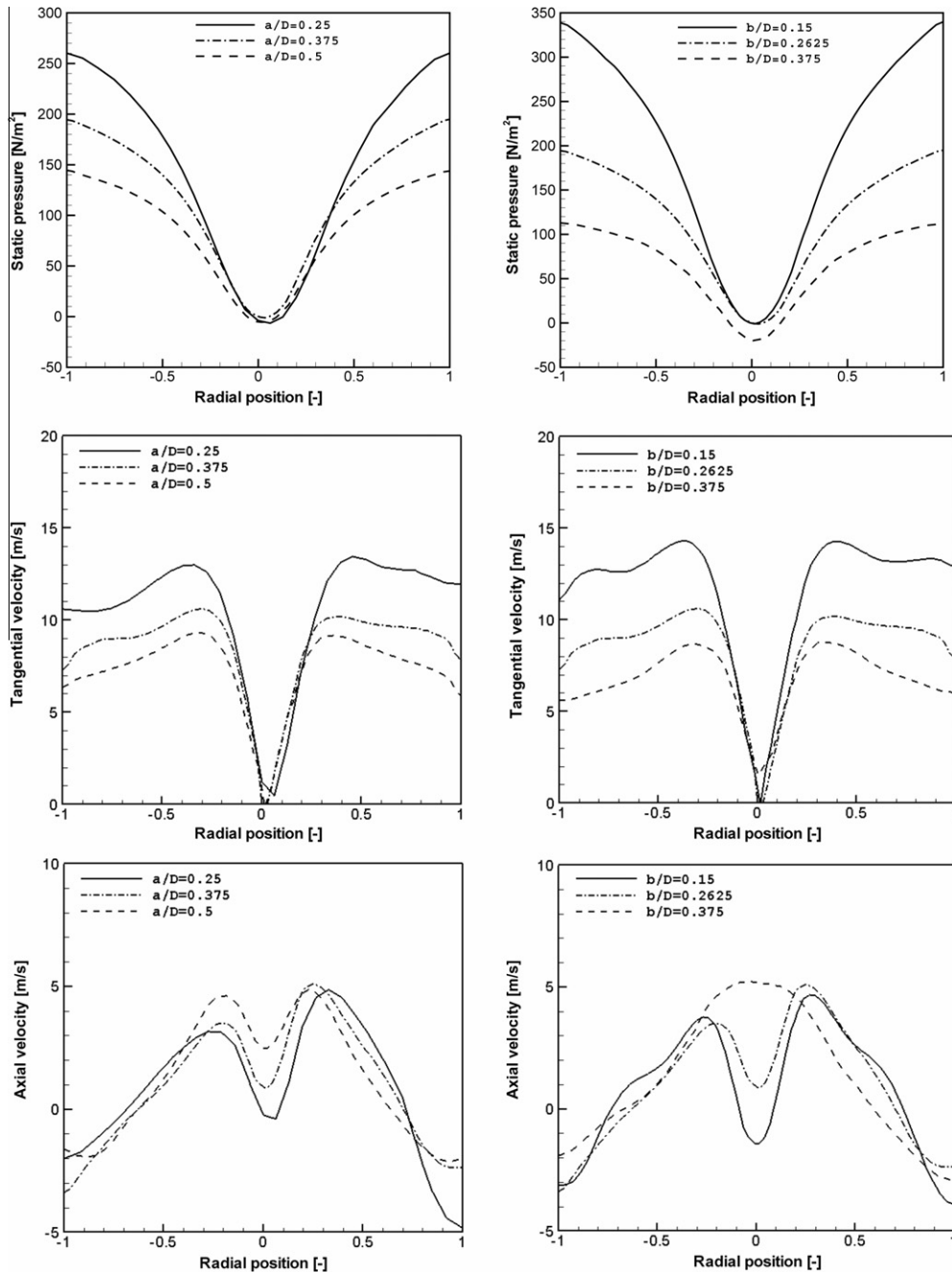
Fig. 6. Comparison between the radial profiles for the time averaged static pressure, tangential and axial velocity at section S9. From top to bottom: static pressure, tangential and axial velocity.

main contributions: (1) the pressure drop at the inlet section (decreased by increasing the inlet dimensions). (2) the pressure drop in the cyclone body due to swirling motion and due to wall friction, this contribution decreases with increasing the cyclone inlet height (as the vortex strength will decrease). (3) the main contribution to the cyclone pressure drop is the energy loss in the exit tube, which mainly depends on the maximum tangential velocity in the cyclone. As is clear from Fig. 6 the maximum tangential velocity decreases with increasing cyclone inlet height, consequently in general the total cyclone pressure drop will decrease with increasing the cyclone inlet height. Fig. 10 also depicts the pressure drop for the three cyclones using four different mathematical models; Muschelknautz method of modeling (MM) [16,58], Casal and Martinez-Benet [11], Shepherd and Lapple [59], Stairmand [60] indicating the same overall trend obtained using RSM simulations for the pressure drop with better matching between the MM model and the current RSM simulation.
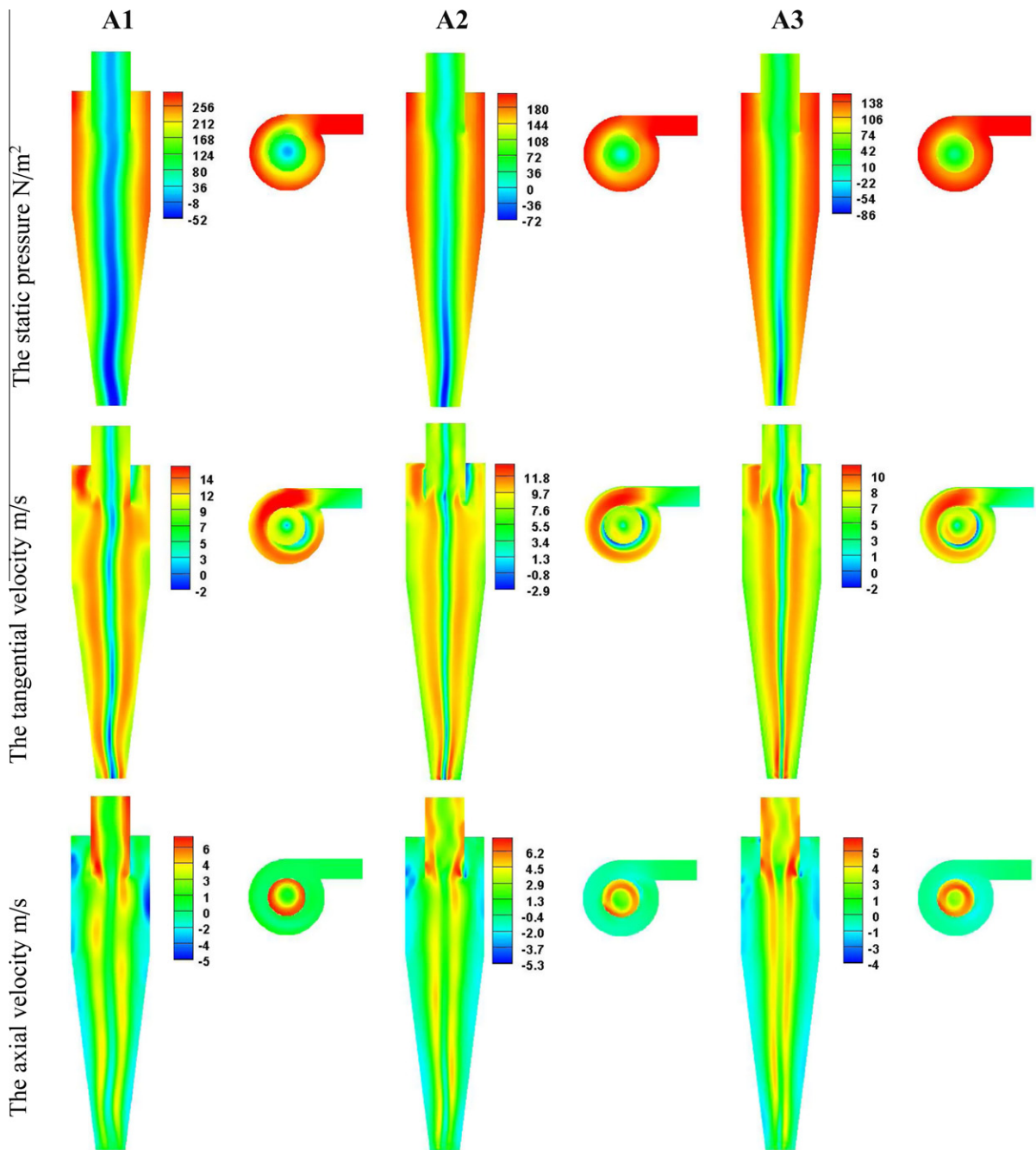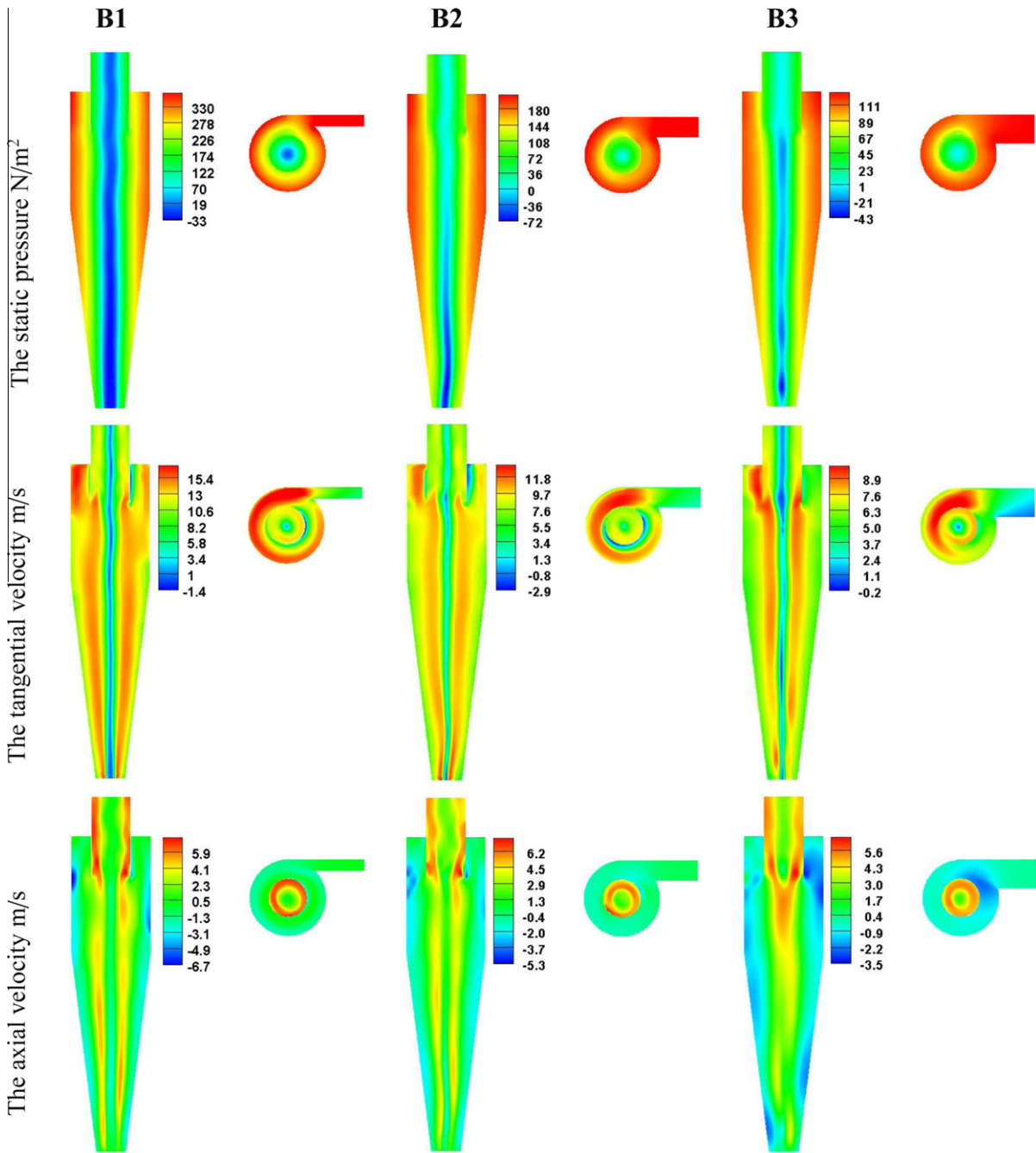
Fig. 7. The contour plots for the time averaged flow variables at sections $Y = 0$ and throughout the inlet section. From top to bottom: the static pressure N/m^2, the tangential velocity m/s and the axial velocity m/s. From left to right cyclone A1 through cyclone A3.

The effect of the cyclone inlet height on the cut-off diameter (particle diameter of 50% collection efficiency) is shown in Fig. 10. The general trend is an increase of the cut-off diameter with increasing cyclone inlet height, due to weakness of the vortex. Fig. 10 also depicts the cut-off diameter for the three cyclones using 2 mathematical models; Iozia & Leith [14] and Rietema [61] indicating the same overall trend obtained using RSM simulations for the cut-off diameter with exact matching between the current RSM results and Rietema model.

4.4.2. The effect of cyclone inlet width

Fig. 10 shows a rapid decrease in the pressure drop when increasing the inlet width for $0.15 \leqslant b/D \leqslant 0.27$ and a smaller decrease for $b/D \geqslant 0.27$. Generally, both the cyclone pressure drop and the cut-off diameter decrease with increasing the

Fig. 8. The contour plots for the time averaged flow variables at sections Y = 0 and throughout the inlet section. From top to bottom: the static pressure N/m², the tangential velocity m/s and the axial velocity m/s. From left to right cyclone B1 through cyclone B3.

cyclone inlet width. The used mathematical models again indicate the same overall trend obtained using RSM simulations for cut-off diameter and pressure drop.

Fig. 10 indicates the need of applying a multi-objectives optimization procedure to get the optimum value for the inlet dimensions. Both the collection efficiency (cut-off diameter) and the pressure drop in cyclone separator are important objective functions to be optimized simultaneously [48]. The effects of changing the cyclone inlet dimensions on pressure drop and collection efficiency are opposite. Increasing the inlet width will save more driving power but leads to reduced collection efficiency (larger cut-off diameter). From the graph, the optimum value will be close to $b/D = 0.25$ with large reduction in pressure drop (energy losses) and small increase in cut-off diameter. Elsayed & Lacor [10] estimated the optimum value for inlet width (b/D) equals 0.236.
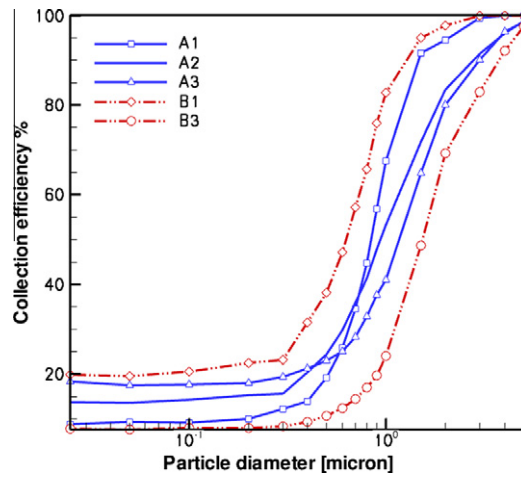
Fig. 9. The Grade efficiency curves for the five cyclones.
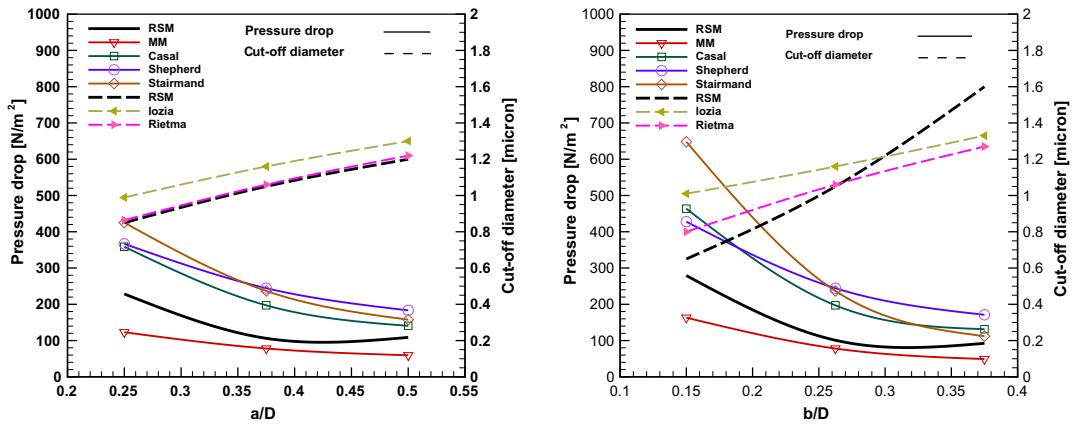

Fig. 10. The effect of inlet dimensions on the pressure drop and cut-off diameter using CFD simulations and different mathematical models.
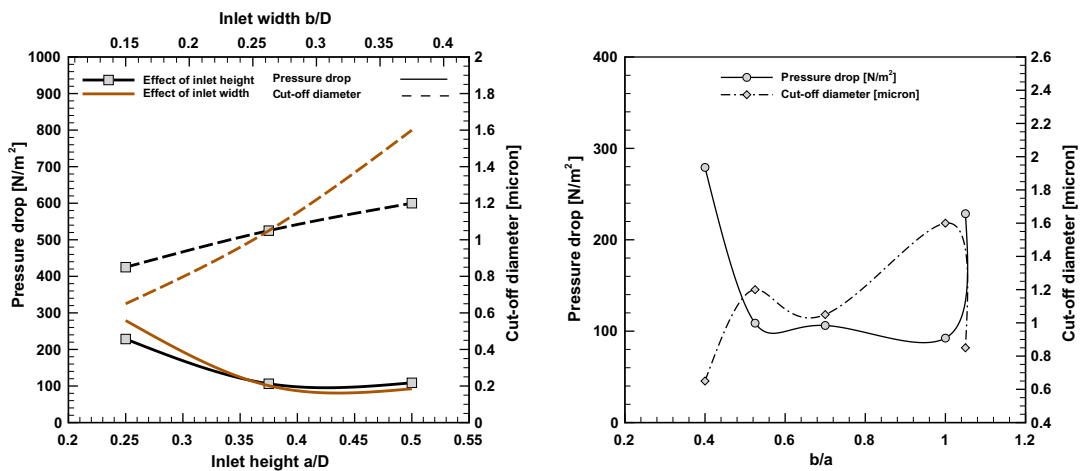

Fig. 11. Comparison between the effect of inlet height and width on the pressure drop and cut-off diameter using CFD simulations.

4.4.3. Inlet height versus inlet width

Fig. 11 shows that, The impact of changing either the inlet height or width on the pressure drop is almost the same. However, The effect of changing the inlet width on the cut-off diameter is more significant in comparison with that of the inlet height. When plot the pressure drop against the ratio of inlet width to inlet height, It becomes clear the optimum range of b/a is from 0.5 to 0.7.

5. Conclusions

Five cyclones of different inlet width and height have been simulated using Reynolds stress model (RSM), to study the effect of cyclone inlet dimensions on the cyclone separator performance and flow pattern. The following conclusions have been obtained.

- The maximum tangential velocity in the cyclone decreases with increasing both the cyclone inlet width and height.
- No acceleration occurs in the cyclone space (the maximum tangential velocity nearly constant throughout the cyclone). Also the variation of both the static pressure and axial velocity in the axial direction is very limited.
- Increasing the cyclone inlet width or height decreases the pressure drop at the cost of increasing the cut-off diameter. So an optimization procedure is needed to estimate the optimum value of inlet dimensions.
- Wider inlet cyclones ($b/D>$ gap between the cyclone barrel and the vortex finder are not preferred.
- The effect of changing the inlet width on the cut-off diameter is more significant in comparison with that of the inlet height.
- The optimum ratio of the inlet width to the inlet height b/a is from 0.5 to 0.7.

As a recommendation of future work, the same study is to be performed but at different flow rates and different particle densities. Also the effect of increasing the cyclone inlet dimensions on natural vortex length and precessing vortex core needs more investigation.

References

[1] A.J. Hoekstra, J.J. Derksen, H.E.A. Van Den Akker, An experimental and numerical study of turbulent swirling flow in gas cyclones, Chemical Engineering Science 54 (1999) 2055–2065.
[2] G. Solero, A. Coghe, Experimental fluid dynamic characterization of a cyclone chamber, Experimental Thermal and Fluid Science 27 (2002) 87–96.
[3] L.Y. Hu, L.X. Zhou, J. Zhang, M.X. Shi, Studies on strongly swirling flows in the full space of a volute cyclone separator, AIChE Journal 51 (3) (2005) 740–749.
[4] P.A. Yazdabadi, A.J. Grifflths, N. Syred, Characterization of the pvc phenomena in the exhaust of a cyclone dust separator, Experiments in Fluids 17 (1994) 84–95.
[5] T. O'Doherty, A.J. Griffiths, N. Syred, P.J. Bowen, W. Fick, Experimental analysis of rotating instabilities in swirling and cyclonic flows, Developments in Chemical Engineering and Mineral Processing 7 (1999) 245–267.
[6] B. Zhang, S. Hui, Numerical simulation and PIV study of the turbulent flow in a cyclonic separator, in: International Conference on Power Engineering, Hangzhou, China, 2007.
[7] W.D. Griffiths, F. Boysan, Computational fluid dynamics (CFD) and empirical modelling of the performance of a number of cyclone samplers, Journal of Aerosol Science 27 (2) (1996) 281–304.
[8] J. Gimbun, T.G. Chuah, T.S.Y. Choong, A. Fakhru'l-Razi, A CFD study on the prediction of cyclone collection efficiency, International Journal for Computational Methods in Engineering Science and Mechanics 6 (3) (2005) 161–168.
[9] J. Gimbun, T. Chuah, A. Fakhru'l-Razi, T.S.Y. Choong, The influence of temperature and inlet velocity on cyclone pressure drop: a CFD study, Chemical Engineering & Processing 44 (1) (2005) 7–12.
[10] K. Elsayed, C. Lacor, Optimization of the cyclone separator geometry for minimum pressure drop using mathematical models CFD simulations, Chemical Engineering Science 65 (22) (2010) 6048–6058.
[11] J. Casal, J.M. Martinez-Benet, A better way to calculate cyclone pressure drop, Chemical Engineering 90 (2) (1983) 99–100.
[12] G. Ramachandran, D. Leith, J. Dirgo, H. Feldman, Cyclone optimization based on a new empirical model for pressure drop, Aerosol Science and Technology 15 (1991) 135–148.
[13] D.L. Iozia, D. Leith, Effect of cyclone dimensions on gas flow pattern and collection efficiency, Aerosol Science and Technology 10 (3) (1989) 491–500.
[14] D.L. Iozia, D. Leith, The logistic function and cyclone fractional efficiency, Aerosol Science and Technology 12 (3) (1990) 598–606.
[15] R.M. Alexander, Fundamentals of cyclone design and operation, in: Proceedings of the Australian Institute of Mineral and Metallurgy, 152, 1949, pp. 203–228.
[16] C. Cortés, A. Gil, Modeling the gas and particle flow inside cyclone separators, Progress in Energy and Combustion Science 33 (5) (2007) 409–452.
[17] F. Boysan, B.C.R. Ewan, J. Swithenbank, W.H. Ayers, Experimental and theoretical studies of cyclone separator aerodynamics, IChemE Symposium Series 69 (1983) 305–320.
[18] R. Xiang, S.H. Park, K.W. Lee, Effects of cone dimension on cyclone performance, Journal of Aerosol Science 32 (4) (2001) 549–561.
[19] K.S. Lim, H.S. Kim, K.W. Lee, Characteristics of the collection efficiency for a cyclone with different vortex finder shapes, Journal of Aerosol Science 35 (6) (2004) 743–754.
[20] A. Raoufi, M. Shams, M. Farzaneh, R. Ebrahimi, Numerical simulation and optimization of fluid flow in cyclone vortex finder, Chemical Engineering and Processing 47 (2008) 128–137.
[21] K.S. Lim, S.B. Kwon, K.W. Lee, Characteristics of the collection efficiency for a double inlet cyclone with clean air, Journal of Aerosol Science 34 (8) (2003) 1085–1095.
[22] B. Zhao, H. Shen, Y. Kang, Development of a symmetrical spiral inlet to improve cyclone separator performance, Powder Technology 145 (2004) 47–50.
[23] H. Yoshida, Y. Inada, K. Fukui, T. Yamamoto, Improvement of gas-cyclone performance by use of local fluid flow control method, Powder Technology 193 (2009) 6–14.
[24] B. Zhao, Y. Su, J. Zhang, Simulation of gas flow pattern and separation efficiency in cyclone with conventional single and spiral double inlet configuration, Chemical Engineering Research and Design 84 (2006) 1158–1165.
[25] A. Avci, I. Karagoz, Theoretical investigation of pressure losses in cyclone separators, International Communications in Heat and Mass Transfer 28 (1) (2001) 107–117.

[26] B. Zhao, Experimental investigation of flow patterns in cyclones with conventional and symmetrical inlet geometries, Chemical Engineering & Technology 28 (9) (2005) 969–972. http://dx.doi.org/10.1002/ceat.200500088.
[27] F. Qian, M. Zhang, Effects of the inlet section angle on the flow field of a cyclone, Chemical Engineering & Technology 30 (11) (2007) 1521–4125.
[28] F. Qian, Y. Wu, Effects of the inlet section angle on the separation performance of a cyclone, Chemical Engineering Research and Design 87 (12) (2009) 1567–1572.
[29] S. Movafaghian, J.A. Jaua-Marturet, R. Mohan, O. Shoham, G. Kouba, The effects of geometry, fluid properties and pressure on the hydrodynamics of gas–liquid cylindrical cyclone separators, International Journal of Multiphase Flow 26 (6) (2000) 999–1018.
[30] F.M. Erdal, S.A. Shirazi, Effect of the inlet geometry on the flow in a cylindrical cyclone separator, Journal of Energy Resources Technology 128 (1) (2006) 62–69.
[31] A.J. Hoekstra, Gas Flow Field and Collection Efficiency of Cyclone Separators, Ph.D. thesis, Technical University Delft, 2000.
[32] M. Sommerfeld, C.A. Ho, Numerical calculation of particle transport in turbulent wall bounded flows, Powder Technology 131 (1) (2003) 1–6.
[33] L. Huang, K. Kumar, A.S. Mujumdar, Simulation of a spray dryer fitted with a rotary disk atomizer using a three-dimensional computional fluid dynamic model, Drying Technology 22 (6) (2004) 1489–1515.
[34] S. Bernardo, M. Mori, A. Peres, R. Dionisio, 3-D computational fluid dynamics for gas and gas-particle flows in a cyclone with different inlet section angles, Powder Technology 162 (3) (2006) 190–200.
[35] C. Fredriksson, Exploratory Experimental and Theoretical Studies of Cyclone Gasification of Wood Powder, Ph.D. thesis, Lulea University of Technology, Sweden, 1999.
[36] B. Zhou, B. Fleck, F. Bouak, J. Gauthier, Comparison of swirling effects on ejector performance using four turbulence models, Canadian Aeronautics and Space Journal 46 (4) (2000) 178–182.
[37] T. Chuah, J. Gimbun, T.S. Choong, A CFD study of the effect of cone dimensions on sampling aerocyclones performance and hydrodynamics, Powder Technology 162 (2006) 126–132.
[38] A. Gupta, R. Kumar, Three-dimensional turbulent swirling flow in a cylinder: Experiments and computations, International Journal of Heat and Fluid Flow 28 (2) (2007) 249–261.
[39] I. Karagoz, F. Kaya, CFD investigation of the flow and heat transfer characteristics in a tangential inlet cyclone, International Communications in Heat and Mass Transfer 34 (9-10) (2007) 1119–1126.
[40] G. Wan, G. Sun, X. Xue, M. Shi, Solids concentration simulation of different size particles in a cyclone separator, Powder Technology 183 (2008) 94–104.
[41] A.M. Jawarneh, H. Tlilan, A. Al-Shyyab, A. Ababneh, Strongly swirling flows in a cylindrical separator, Minerals Engineering 21 (5) (2008) 366–372.
[42] F. Kaya, I. Karagoz, Performance analysis of numerical schemes in highly swirling turbulent flows in cyclones, Current Science 94 (10) (2008) 1273–1278.
[43] A. Secchiaroli, R. Ricci, S. Montelpare, V. D'Alessandro, Numerical simulation of turbulent flow in a Ranque–Hilsch vortex tube, International Journal of Heat and Mass Transfer 52 (23-24) (2009) 5496–5511.
[44] R.B. Xiang, K.W. Lee, Numerical study of flow field in cyclones of different height, Chemical Engineering and Processing 44 (2005) 877–883.
[45] J. Gimbun, T. Chuah, T. Choong, Y. Fakhru'l-Razi, Prediction of the effects of cone tip diameter on the cyclone performance, Aerosol Science and Technology 36 (2005) 1056–1065.
[46] K. Elsayed, C. Lacor, The effect of vortex finder diameter on cyclone separator performance and flow field, in: Fifth European Conference on Computational Fluid Dynamics (ECCOMAS CFD10), Lisbon, Portugal, 2010. URL <http://web.univ-ubs.fr/limatb/EG2M/Disc_Seminaire/ECCOMAS-CFD2010/papers/01022.pdf>.
[47] H. Safikhani, M. Akhavan-Behabadi, M. Shams, M.H. Rahimyan, Numerical simulation of flow field in three types of standard cyclone separators, Advanced Powder Technology 21 (4) (2010) 435–442.
[48] H. Safikhani, M. Akhavan-Behabadi, N. Nariman-Zadeh, M.M. Abadi, Modeling and multi-objective optimization of square cyclones using CFD and neural networks, Chemical Engineering Research and Design, Corrected Proof, in press, doi:DOI: doi:10.1016/j.cherd.2010.07.004.
[49] M. Azadi, M. Azadi, A. Mohebbi, A CFD study of the effect of cyclone size on its performance parameters, Journal of Hazardous Materials 182 (1-3) (2010) 835–841.
[50] M.D. Slack, R.O. Prasad, A. Bakker, F. Boysan, Advances in cyclone modeling using unstructured grids, Transaction in IChemE 78 Part A (2000).
[51] B.E. Launder, G.J. Reece, W. Rodi, Progress in the development of a reynolds-stress turbulence closure, Journal of Fluid Mechanics 68 (03) (1975) 537–566.
[52] S.A. Morsi, A.J. Alexander, An investigation of particle trajectories in two-phase flow systems, Journal of Fluid Mechanics 55 (02) (1972) 193–208.
[53] H. Shalaby, On the Potential of Large Eddy Simulation to Simulate Cyclone Separators, Ph.D. thesis, Chemnitz University of Technology, Chemnitz, Germany, 2007.
[54] J. Dirgo, D. Leith, Cyclone collection efficiency: comparison of experimental results with theoretical predictions, Aerosol Science and Technology 4 (1985) 401–415.
[55] A. Benim, K. Ozkan, M. Cagan, D. Gunes, Computational investigation of turbulent jet impinging onto rotating disk, International Journal of Numerical Methods for Heat & Fluid Flow 17 (3) (2007) 284–301.
[56] A. Gorton-Hülgerth, J. Woisetschläger, G. Wigley, G. Staudinger, Investigation of the flow field in the upper part of a cyclone with laser and phase doppler anemometry, Particle and Particle System Characterization 17 (2000) 21–27.
[57] W. Peng, A.C. Hoffmann, P.J.A.J. Boot, A. Udding, H. Dries, A. Ekker, J. Kater, Flow pattern in reverse-flow centrifugal separators, Powder Technology 127 (2002) 212–222.
[58] M. Trefz, E. Muschelknautz, Extended cyclone theory for gas flows with high solids concentrations, Chemie Ingenieur Technik 16 (1993) 153–160.
[59] C.B. Shepherd, C.E. Lapple, Flow pattern and pressure drop in cyclone dust collectors cyclone without intel vane, Industrial & Engineering Chemistry 32 (9) (1940) 1246–1248.
[60] C.J. Stairmand, The design and performance of cyclone separators, Industrial and Engineering Chemistry 29 (1951) 356–383.
[61] K. Rietema, Het mechanisme van de afscheiding van fijnverdeelde stoffen in cyclonen, De Ingenieur 71 (39) (1959) ch59–ch65 ((in dutch)).